Arch. Metall. Mater. **69** (2024), 3, 987-996

DOI: https://doi.org/10.24425/amm.2024.150919

M. ALHARBI[1], H. ALTHUBYANI[2], E. ALARFAJ[1], D. DASTAN[3*], A. TIMOUMI[2*], L. TAO[4], H. ALBETRAN[5], Ş. ŢĂLU[6*]

PHOTOCATALYTIC PERFORMANCES OF DIP-COATED Ag DOPED TiO_2 THIN FILMS

In this study, dip coating technique is used to deposit titanium dioxide (TiO_2) and silver (Ag)–doped–TiO_2 nanocomposite thin films on glass substrates. The obtained films are typified using different characterization techniques such as X-ray diffraction (XRD), and UV–Vis-NIR spectroscopy. Films are also tested for environmental applications related to color degradation (methylene blue). The XRD analysis confirms that the prepared nanostructures are the anatase phase of titania. The crystal sizes of annealed Ag–TiO_2 as well as TiO_2 thin films have been summarized across the XRD pattern and are approximately 29±1 and 23±1 nm, respectively. Additionally, the energy bandgaps of the photocatalysts (Pure–TiO_2 and Ag–TiO_2) are found to be around 3.3 and 3.02 eV, respectively. The photocatalytic activity of TiO_2 and Ag-doped TiO_2 nanocomposite thin films is tested in the same initial concentrations of methylene blue in water (3×10^{-5} M). The photodegradation behavior of Ag–TiO_2 (3% by weight) shows a good improvement against pure TiO_2 for the concentrations of methylene blue in the pseudo-first order Langmuir-Hinshelwood (LH) model of the kinetics reaction. The global pseudo-first order reaction constant, k, for these concentrations goes from less than 1.4×10^{-3} min^{-1} for TiO_2 films to 5.4×10^{-3} min^{-1} for Ag–TiO_2 films. This improvement is due to the incorporation of Ag, which increases the lifetime of the electrons and the separated holes, that decreases the rate of recombination (electron-hole) and which also generates reactive oxygen species. These features open the route to future applications for photocatalytic wastewater treatment and environmental remediation under solar irradiation.

Keywords: Dip Coating; Methylene Blue; Photocatalytic; Photodegradation; TiO_2

1. Introduction

In the last years, the contamination of water and air by chemical pollutants has been growing rapidly. Several studies are carried out to use semiconductor photocatalysis to remove these pollutants [1-10]. Photocatalysis can be divided into two categories; non-photochemical and photochemical [11-15]. The photocatalysis process can produce potent chemical oxidants known as reactive oxygen species (ROS) [16], subsequently speeding up the oxidation of pollutants. The photocatalysis process that uses various solid semiconductors is a heterogeneous process that has many good advantages as a low-cost, high efficiency, low energy consumption and environmentally friendly [17,18]. Generally, semiconductors included TiO_2, WO_3, CdS, CeO_2, ZnO, Fe_2O_3, SnO_2, MoO_3, ZrO_2, and ZnS are chosen as photocatalysts as a result of their narrow band gap and distinguished electronic configuration [19-35].

TiO_2 has a significant importance between all metal oxides which is developed for photocatalysis applications as it has received great attention due to its chemical stability and high reactivity under UV light rays ($\lambda < 390$ nm) [20,25,29]. Recently, studies have shown that TiO_2 nanostructures are more effective such as nanoparticles, thin films [20,25,29,36], and nanofibers [37]. Unfortunately, due to the wide gap of TiO_2 (3.2 eV), it can only be applied in the ultraviolet region of the solar spectrum which accounts for 5% of solar energy while visible light constitutes 45% of solar energy [20,25,38-39]. The efficiency of TiO_2 can be enhanced by alteration of surface, as there are many ways to modify the surface of titanium dioxide among which dye sensitization [40], coupled semiconductor systems [41],

[1] QASSIM UNIVERSITY, DEPARTMENT OF PHYSICS, COLLEGE OF SCIENCES, BURAYDAH ALMOLAYDAH, BURAYDAH, SAUDI ARABIA
[2] UMM AL-QURA UNIVERSITY, FACULTY OF APPLIED SCIENCE, PHYSICS DEPARTMENT, MAKKAH, P.O. BOX 715, SAUDI ARABIA
[3] CORNELL UNIVERSITY, DEPARTMENT OF MATERIALS SCIENCE AND ENGINEERING, ITHACA, NEW YORK, 14850, USA
[4] UNIVERSITY OF SCIENCE AND TECHNOLOGY LIAONING, SCHOOL OF CHEMICAL ENGINEERING, ANSHAN 114051, CHINA
[5] IMAM ABDULRAHMAN BIN FAISAL UNIVERSITY, DEPARTMENT OF PHYSICS, COLLEGE OF SCIENCE, P.O. BOX 1982, DAMMAM 31441, SAUDI ARABIA
[6] TECHNICAL UNIVERSITY OF CLUJ-NAPOCA, THE DIRECTORATE OF RESEARCH, DEVELOPMENT AND INNOVATION MANAGEMENT (DMCDI), CONSTANTIN DAICOVICIU ST., NO. 15, CLUJ-NAPOCA, 400020, CLUJ COUNTY, ROMANIA

* Corresponding authors: d.dastan61@yahoo.com, aotemoume@uqu.edu.sa, stefan.talu@auto.utcluj.ro

inclusion of nonmetal ions, as well as impurity doping of TiO_2 with transition metal ions and noble metal ion [42].

The efficiency of photocatalysis can be enhanced by depositing some noble metals such as Ag, Pt, Au, Pd on the TiO_2 surface in various ways including trapping electrons thus preventing the formation of e/h pairs and enhancing the electron hole [43-47]. Ag has many characteristics that distinguish it from other noble elements such as high efficiency and low price compared to other noble metals in addition to antimicrobial properties [48], and high oxygen adsorption reactivity [49]. For these reasons a considerable interest is given to Ag metal doping of TiO_2 thin films.

In this work, silver was selected to modify the TiO_2 surface as a photocatalyst in thin film form and select Methylene blue as pollutant in aqueous solutions. There are several advantages for the use of silver modified TiO_2 as a photocatalyst [50,51], but some disadvantages are also pointed out [52]. There are many researches are performed on photocatalytic activity of TiO_2 and some on the removing of methylene blue [53], but there are a limited number of researches on the combination of silver modified TiO_2 and Methylene blue. Methylene blue is well known to be a widely used as an organic toxic dye in a range of different fields, which can cause environmental contaminations to harm environment and human health [35]. Therefore, any novel developments in the methods of degrading Methylene blue are very important.

In the recent years, many methods have been developed for processing TiO_2 thin films among them electron beam evaporation [54], chemical vapor deposition [55], spin coating technique [56-59], atmospheric pressure chemical vapor deposition [60] and sol-gel method [21-24,61,62]. The sol-gel dip-coating process is particularly suitable for the preparation of vitreous or polycrystalline films that need excellent homogeneity, purity, and uniformity on any substrate types [58,59]. In this research, pure TiO_2 and Ag−doped TiO_2 transparent thin films supported on a glass substrate are prepared using the dip coating method. The activity properties of the photocatalyst before and after surface modification with metallic Ag for the degradation of methylene blue are examined. Titanium dioxide is presented as a thin film, and its efficiency as a UV photocatalytic is tested. Titania efficiency as a photocatalytic is studied and the efficiency results of the samples are compared.

2. Methods

2.1. Materials and devices

For this work, all the employed chemicals are of analytical reagent grade and used without further purification. The dip coating method is used for the preparation of TiO_2−based sol-gel solutions. The list of different chemical materials utilized for this method with their properties are listed in TABLE 1.

TABLE 1

The chemical materials and solvents utilized for synthesis of pure−TiO_2

Chemicals	Formula	Molecular Weight (g/mol)	Density (kg/m^3)
Titanium Isopropoxide	$C_{12}H_{28}O_4Ti$	284.22	960
Isopropanol	C_3H_8O	60.10	790
Acetic Acid	$C_2H_4O_2$	60.05	1049
Methanol	CH_4O	32.04	792
Silver nitrate	$AgNO_3$	169.87	4350
Deionised water	H_2O	18.015	1000
Methylene blue	$C_{16}H_{18}ClN_3S$	319.85	1757

For the sample preparation, Hitter stirrer (SH_2), a controlled temperature, Dip coater (Ni–Lo–Dip cotter), a controlled speed (speed up and speed down at 99.99 mm/min max), Ultrasonic (Digital ultrasonic cleaner), and an Infrared light lamp (300 W) with voltage 220 V were used.

2.2. Preparation of Pure and Ag doped TiO_2 solution

The materials (beakers- graduated cylinder- graduated pipette) were successively immersed into ultrasonic of acetone (100 ml), isopropanol (100 ml), methanol (100 ml) and deionised water (100 ml) for cleaning, and each for 20 min. The method utilized in this study follows the one utilized in the reference 76. The solution of pure TiO_2 was prepared according to following steps [61]:

- 3.2 ml titanium isopropoxide was poured into beaker.
- 9.3 ml isopropanol was added drop by drop to titanium isopropoxide by graduated pipette.
- The solution was left under closed agitation under heating at 62°C for 10 min.
- 10.3 ml acetic acid was poured to the solution by graduated pipette under closed agitation under heating at 62°C for 15 min. We note the solution was changed to gel with white color after 13 munities through this step.
- 24 ml methanol was added to the solution by graduated pipette under closed agitation under heating at 62°C for 15 min. We note that the solution color was changed to white color after methanol was added to the solution.
- The solution was left under closed agitation for 2 h.
- The solution was left under closed under room temperature for 24 h.

Two solutions were prepared for the preparation of the solution Ag-doped TiO_2. The first included 1 mol of titanium isopropoxide, 2 mol of glacial acetic acid and 2 mol of isopropanol under heating at 62°C for 15 min under closed agitation. The second has consisted of silver nitrate (3% from its molecular weight) was dissolved it in a 1 mol of methanol, 2 mol of glacial acetic acid and 2 mol of isopropanol. The second solution was added to the first solution by graduated pipette under closed agitation. The solution was left under closed agitation for 2 h then was left it under closed under room temperature for 24 h.

2.3. Preparation of Samples for Photocatalysis

Glass plate's substrates with dimensions of (20×100 mm) were used to prepare samples for photocatalysis process. The glass plate substrates are cleaned by Ultrasonic baths. Firstly, the substrates were successively immersed into Ultrasonic baths of (acetone, isopropanol, methanol, and Deionized water) for 20 min each, after that they were dried by Nitrogen gas for 1 min and finally, they were also dried by infrared lamp for 10 min. The TiO_2 films are deposited on the glass substrates using the dip-coating technique. The glass substrate was immersed in the TiO_2 sol-gel, and then left in the solution for 5 s to end the substratum long contact time with the coating solution for full wetting. The substrate was then withdrawn vertically at a constant speed of 2 mm/s (Fig. 1). Infrared light lamp (300 W with voltage 220 V) dried the coated sample for 2 min. To get the required thickness, the above steps were repeated several times. The coated surface area was 2×2 cm. The coated samples with pure TiO_2 and Ag-doped TiO_2 solution and deposited on glass substrates underwent annealing process at 400°C for 60 min in the air. The annealing cycles were chosen to obtain the dominant photo-catalytic films needed for the anatase process. The temperature was ramped up 5°C/min, then held constant at 400°C for an hour, and finally ramped down 5°C/min. Typical heating and cooling cycles are done by a furnace (NEYTECH Qex). Such samples were placed in a clean, cool, and dry container and used in aqueous solution as photocatalysts for photodegradation of Methylene Blue (MB).

2.4. Photocatalytic Degradation of Methylene Blue (MB)

The photocatalytic reactor system consists of a glass reactor beaker with an effective volume of 200 mL. Photo-irradiation was performed using a UV lamp pattern (UVGL–58 MINER ALIGHT Lamp) mounted outside the core reactor vessel. The hand lamp contains 6 watt tubes that provide high intensity, long wave or short wave ultraviolet light. Typical intensities for shortwave are 1300 μW/cm² at 7.62 cm; for long waves: 350 μW/cm² at 15.24 cm. The unit has an on/off push button switch for each tube and a sturdy, convenient handle. The case is made from sturdy plastic. The lamp can be used with the 19-1943 stand or the 17-1725 Chromato-Vue cabinet. The dimensions are (37.46×8.89×6.66) cm for operation on 115 volts, 60 Hz, AC. The gap from thin films to the light source was 12 cm. The system also consists of oxygen gas which pumped at a slow flow rate in the bottom of the reactor to obtain oxygen uniformly distribution into the solution. Thin films of titanium were placed vertically inside the solution so that they face the light source to obtain high illuminated area of the photocatalyst surface. Solution of methylene blue with a concentration of 10 ppm were obtained by following way: 0.002 g from methylene blue powder was obtained by digital weighing balance, then it was mixed with 100 mL of distilled water and then 20 ml from solution of methylene blue were obtained and mixed with 200 mL of distilled water. Finally, the concentration of methylene blue was 3×10^{-5} M in the solution.3ml of the solution was obtained before irradiation to measure optical absorption which was recorded as a 0-s absorption (initial concentration). The solution is irradiated under ultraviolet for three hours. The degradation reaction is closely monitored by calculating UV absorption spectra for pure TiO_2 thin film every hour and for Ag-doped TiO_2 every 30 min. The mechanism of photocatalysis for the disintegration of MB using Ag/TiO_2 nanocomposites was described through the following equations:

$$\mathrm{Ag-TiO_2} + h\nu \rightarrow \mathrm{Ag-TiO_2}(CBe^-) + \\ + \mathrm{Ag-TiO_2}(VBh^+) \quad (1)$$

$$\mathrm{Ti^{3+}} \rightarrow \mathrm{Ti^{4+}} + e^- \quad (2)$$

$$h^+ + \mathrm{H_2O} \rightarrow \mathrm{OH^\bullet} \quad (3)$$

$$e^- + \mathrm{Ag} \rightarrow \mathrm{Ag^-} \quad (4)$$

$$\mathrm{Ag^-} + \mathrm{O_2} \rightarrow \mathrm{{}^\bullet O_2^-} \quad (5)$$

$$\mathrm{{}^\bullet O_2^-} + e^- + 2\mathrm{H^+} \rightarrow \mathrm{H_2O_2} \quad (6)$$

$$\mathrm{{}^\bullet H_2O_2} + e^- \rightarrow \mathrm{OH^\bullet} + \mathrm{{}^-OH} \quad (7)$$

$$MB/MB^\bullet + \mathrm{OH^\bullet} \rightarrow Dgradation\ products \quad (8)$$

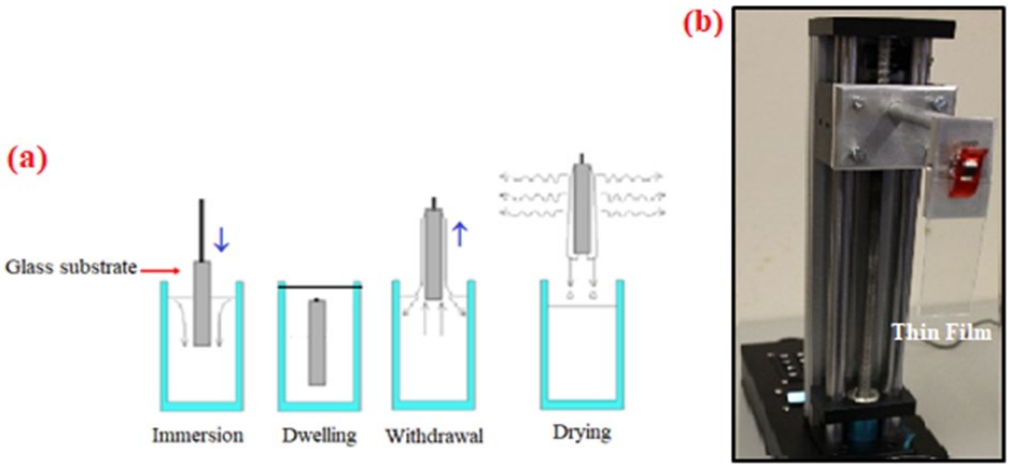

Fig. 1. TiO_2 thin film deposition process (a) and obtained thin film on glass substrates (b)

The free radical trapping experiments indicate that the photogenerated h^+ and $^{\bullet}O_2^-$ are the two main active substances for photocatalytic degradation. It is concluded that the most important radicals to degrade MB solution are ranked as follows:

$$h^+ > {}^{\bullet}O_2^- > e^- > OH^{\bullet}.$$

2.5. Characterization Technique

Synthesized samples were characterized by X-ray diffraction (XRD), the optical absorption was examined with a UV-Vis Spectrometer (UV-Vis, Jasco J-815).

3. Results and discussion

3.1. XRD Characterization of Pure and Ag-doped TiO_2 Thin Films

XRD spectra were used to examine the fabricated TiO_2 phase configuration and Ag doped TiO_2 photocatalyst. Fig. 2a, b displays the XRD spectra for the produced TiO_2 thin film with Ag–TiO_2 photocatalysts and after deposited onto glass slides by Dip Coating System – (Ni – Lo – Dip coater) and annealed at 400°C in air atmosphere. As shown in Fig. 2a, b, the anatase phase appears in the pure TiO_2 and the doped one appears in thin film form. Observing clearly, the anatase crystalline phases having almost similar peaks which are marked on the XRD pattern. Anatase (JCPDS Card no. 21-1272) peaks are depicted with 2θ angles of 25.2°, 36.1°, 48.1°, 54.2°, and 62.4° which are related to the Miller indices of (101), (004), (200), and (211), (204) on the crystal planes accordingly [63-65]. It indicates that the Ag incorporation hardly alter the Ag–TiO_2 photocatalyst crystal structure. The Ag peaks cannot be distinguished clearly from the TiO_2 peaks. Reasons can be better ascribed to a well and proper spreading of the Ag particles in the thin film matrix of TiO_2, It is likely that the metal oxide atoms are not well dispersed in the top layer. The crystalline sizes of annealed Ag–TiO_2, as well as the TiO_2 thin films, are summed up through the XRD pattern by applying Scherer equation [49] which are 29±1 and 23±1 nm respectively and these values are obtained from the peak (101).

3.2. UV-Vis Absorption Spectra in Pure–TiO_2, and Ag–TiO_2 Films

To monitor the effect of Ag incorporating onto the TiO_2 thin films photocatalysts, Fig. 3 shows UV-vis absorption spectra in pure–TiO_2, and Ag–TiO_2 films supported on slides glass around the bounds of 300 to 600 nm as the active substance. The UV-vis absorption spectra reveal that the Ag–TiO_2 photocatalyst absorption edges are properly expanded to the visible region. Also, Ag–TiO_2 films absorbance is moderately moved to the visible region when compared to the pure–TiO_2 photocatalyst. The visible region absorption movement is adduced to the surface plasmon reaction of Ag nanoparticles over the pure–TiO_2 thin films.

The following equation was used to determine the band gaps of the composite films [44,46,66-69]:

$$(\alpha h\nu)^2 = A(h\nu - E_g) \tag{9}$$

where α, h, Eg, A, and v, are the absorption coefficient, Planck constant, proportionality constant, bandgap, and incident light frequency, respectively. The plot of $(\alpha h\nu)^2$ vs photon energy ($h\nu$) observed in Fig. 4b is used to analyze the energy band gaps of the

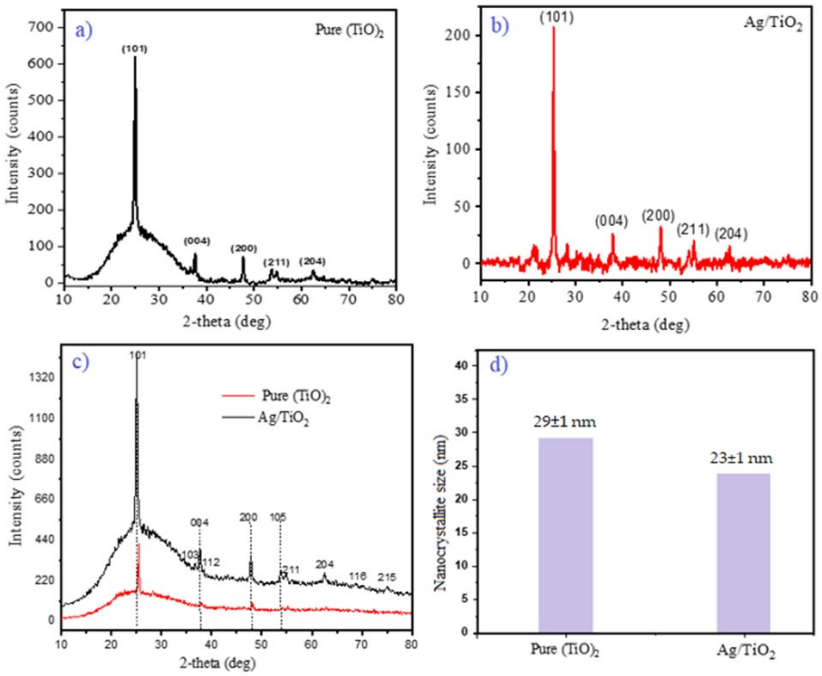

Fig. 2. X-ray diffraction patterns for (a) pure TiO_2 thin film, (b) Ag–TiO_2 photocatalysts annealed up 400°C within 1h in air atmosphere, (c) combined and indexed graphs and (d) nanocrystallite size

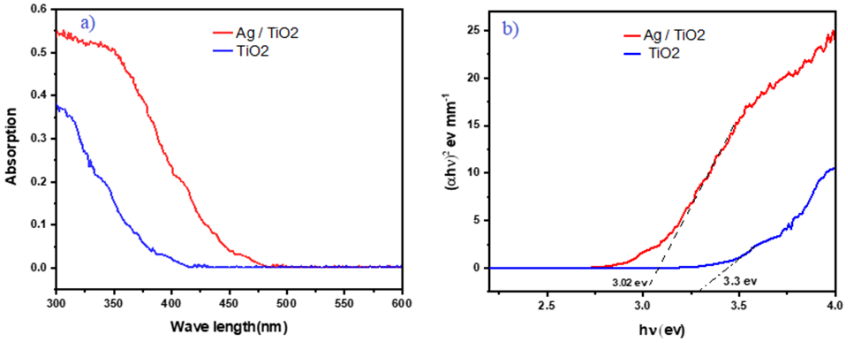

Fig. 3. UV-vis absorption and Tauc plots of (a) pristine Pure–TiO_2, and (b) Ag–TiO_2 photocatalysts composite films

Pure-TiO_2, and Ag–TiO_2 photocatalysts. The pristine TiO_2 photocatalyst has a **band gap of around 3.3 eV**, while the band gap of Ag–TiO_2 photocatalyst is 3.02 eV. Furthermore, the pure–TiO_2 and Ag–TiO_2 photocatalysts valence band (V_B) and conduction band (C_B) are assessed using the following equation [70, 71]:

$$E_{CB} = \chi - 0.5E_g,\ E_{VB} = E_{CB} + E_g \qquad (10)$$

While χ represents the semiconductor's absolute electronegativity, with the χ value of TiO_2 being 5.9 eV [72]. E_e is the free electrons energy using the hydrogen scale (about 4.5 eV). The E_{CB} and E_{VB} for TiO_2 and Ag–TiO_2 were measured as –0.25, +3.05, –0.11, and 2.91 eV, consecutively.

3.3. Analysis of MB Solution UV-vis Absorption Using the Pure TiO_2 and Ag-Doped TiO_2 Thin Film

Fig. 4 shows the methylene blue (MB) solution optical absorption spectra, photo degradation by pure–TiO_2 thin film, which was annealed at 400°C, a key factor of time irradiation. Clearly, the absorption spectra revealed a dual-peak characteristic at 664 and 615 nm, corresponding to monomers and dimers, consecutively [44,46,73]. During irradiation, owing to hypochromic effect [71,74] at 664 nm the peak developed a progressively blue shift into shorter wavelength (Fig. 5) which indicates the photo degradation of MB. Nonetheless, the concentration of MB solution quite does not change for all measurement in the presence of TiO_2 film at dark conditions. As shown, dye concentration progressively reduces with the photo-reaction time. Despite after 120 min of reaction time, there is no observation of the photocatalysts deactivation. TABLE 2 shows the MB degradation. The apex degradation of MB solution is observed at 83.4% after 8 h which has some amount of the pure–TiO_2 film annealed at 400°C. Fig. 5 shows the methylene blue (MB) solution optical absorption spectra, photo degradation by the Ag–TiO_2 thin film which was annealed at 400°C for 1 h as a key factor of the UV irradiation time. The reaction rate for Ag–TiO_2 films has been observed to significantly increase. A clear decrease in the absorbance from the concentration of 3×10^{-5} M at zero time to 1.6×10^{-5} M after two hours. TABLE 3 shows the MB degradation. The apex degradation of MB solution is observed at 86.9% after 4 h which has some amount Ag–TiO_2 thin film annealed at 400°C.

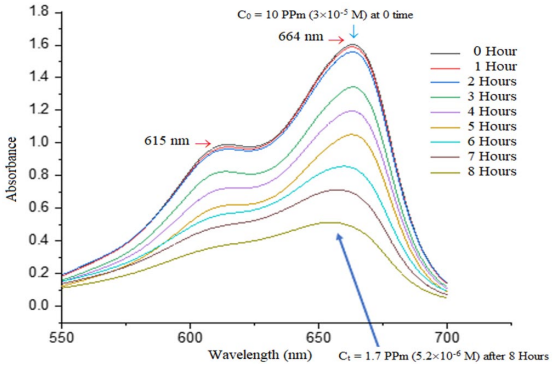

Fig. 4. The Optical absorption of Methylene Blue (MB) after the photocatalysis process for different exposure times by use TiO_2 thin films

TABLE 2

The degradation MB showing first-order rate constants (k) and the C_t concentration of methylene blue (MB) at t time for TiO_2 thin films

No.	Time (t) (min)	C_t (M)	K_{app} (min^{-1})	D (%)	C_t/C_0	$\ln(C_t/C_0)$
1	0	3×10^{-5}	—	0%	1.0	0
2	60	2.9×10^{-5}	6.3×10^{-4}	7%	0.97	–0.03
3	120	2.6×10^{-5}	1×10^{-3}	16%	0.87	–0.14
4	180	2.33×10^{-5}	1.2×10^{-3}	25.3%	0.77	–0.26
5	240	2×10^{-5}	1.5×10^{-3}	34.3%	0.67	–0.40
6	300	1.66×10^{-5}	1.8×10^{-3}	53.2%	0.55	–0.60
7	360	1.36×10^{-5}	1.9×10^{-3}	56.4%	0.45	–0.80
8	420	9.6×10^{-6}	2.5×10^{-3}	69.3%	0.32	–1.14
9	480	5.2×10^{-6}	3.3×10^{-3}	83.4%	0.17	–1.80

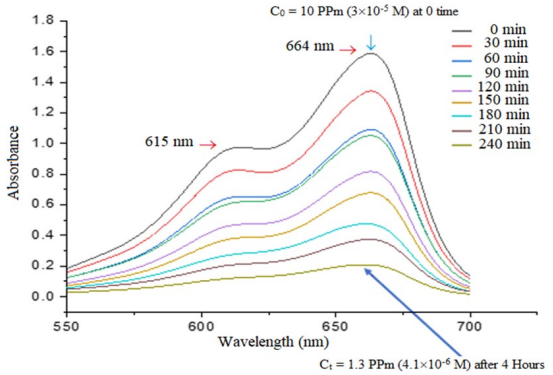

Fig. 5. The Optical absorption of Methylene Blue (MB) after the photocatalysis process for different exposure times by use Ag–TiO_2 thin films

TABLE 3

The degradation MB showing first-order rate constants (K) and the C_t concentration of methylene blue (MB) at t time for Ag–TiO_2 thin films

No.	Time (min)	C_t (M)	K_{app} (min^{-1})	D (%)	C_t/C_0	$\ln(C_t/C_0)$
1	0	3×10^{-5}	—	0	1	0.00
2	30	2.64×10^{-5}	5.6×10^{-3}	15.5%	0.88	–0.13
3	60	2.3×10^{-5}	5.1×10^{-3}	26.5%	0.76	–0.27
4	90	2×10^{-5}	5×10^{-3}	36%	0.67	–0.40
5	120	1.63×10^{-5}	5.6×10^{-3}	48.8%	0.53	–0.64
6	150	1.34×10^{-5}	5.6×10^{-3}	57%	0.45	–0.80
7	180	9.3×10^{-6}	6.7×10^{-3}	70.2%	0.31	–1.20
8	210	7.4×10^{-6}	6.9×10^{-3}	76.3%	0.25	–1.40
9	240	4.1×10^{-6}	8.5×10^{-3}	86.9%	0.13	–2.04

Fig. 6 shows the C_t/C_0 (methylene blue) as a function of time under UV irradiation, with the inclusion of pure–TiO_2 and Ag–TiO_2 thin films within 30-480 min. Similar profile to the characteristics was seen in Fig. 6 for different dyes photocatalytic degradation; earlier literatures showed that the degradation rates of photocatalyst of textile dyes in heterogeneous photocatalytic oxidation systems under UV light illumination followed Langmuir-Hinshelwood (L-H); the Langmuir-Hinshelwood expression which analyzes the kinetics of heterogeneous catalytic systems is depicted by [75,76]:

$$r = -\frac{dC}{dt} = \frac{k_t K[C]}{1 + K[C]} \tag{11}$$

Where r is the mineralization of dye rate, k_t is the rate constant, C is the concentration of methylene blue, and K is the coefficient of adsorption. The equation (1) can be solved succinctly for (t) via making some changes in [MB] at the initial concentration to a zero benchmark point as follows:

$$-\frac{dC}{dt} = k_t K \tag{12}$$

Integration of (1):

$$[C] = [C]_0 e^{-k_{app}t} \tag{13}$$

$$\ln\left(\frac{[C]_t}{[C]_0}\right) = -K_{app}t \tag{14}$$

Where (t) represents time in minutes, k_{app} (k_tK) is the apparent reaction rate constant (min^{-1}), and C_t is the MB of concentration at each time. (L-H) kinetics equation which commonly is applied in explaining the kinetic processes of the heterogeneous catalyst; a pseudo-first-order kinetic model presumption was in several literatures used in explaining the outcomes of the various condition of the experiment [77]. Fig. 6 depicts a little decrease in the concentration of MB (about 16%), when subjected to UV radiation for 2 h using TiO_2 pure thin films. These are anticipated results because TiO_2 thin films are highly active photo-catalyst using this type of radiation. A typical behavior is visible for TiO_2 owing to its wide band gap [78].

Fig. 7 displays how Ag–TiO_2 thin films exhibit a vital rise in the photocatalytic activity, where the concentration of MB is decreased (about 49%), when it was subjected to UV radiation for 2 h. These results can be attributed to silver aggregates that can accumulate charges on the surface of TiO_2 as well as to accepting of electrons within the semiconductor.

While electrons accumulation can decrease the carrier's recombination, and expanding the generation of reactive oxygen types and apart from the possibility of changes on the Ag doped on TiO_2 and a combined oscillation can be produced, termed as (SPR) Localized Surface Plasmon Resonance [79]. Other studies have shown that the oscillation of the electrons in the conduction band of silver particles is collective, and this suggests the possibility of the increase in photocatalytic activity due to the relationship between the semiconductor and the metal [80]. Pseudo-first-order model is used in the data kinetics of Fig. 7.

It is important to note that the slope is obtained from of the linear fitting of ln C_t/C_0 vs (t) values for each test. Ag–TiO_2 thin films have a k_{app} value of 5.4×10^{-3} min^{-1}; this value is 4 times greater than the k_{app} value 1.4×10^{-3} min^{-1} of TiO_2 thin films. From the k_{app} values obtained it is concluded that the photo reduction method is productive which demonstrated that this process could be applied as a substitute in enhancing the photocatalytic activity of TiO_2 using UV light irradiation. TABLE 4

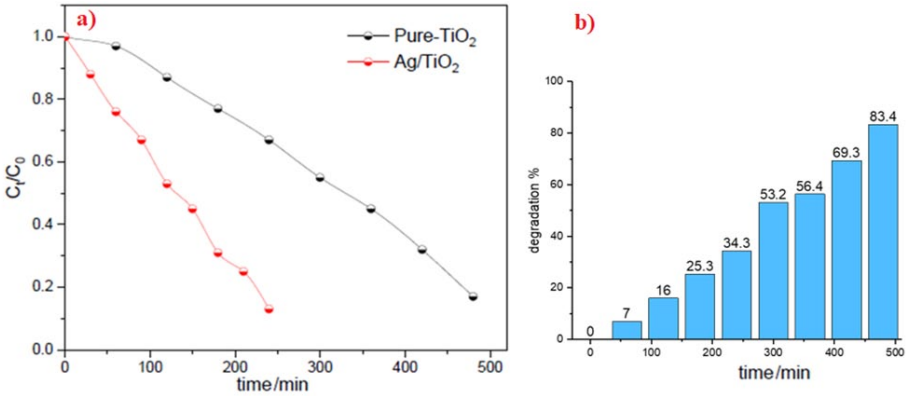

Fig. 6. a) (C_t/C_0) vs (t) using UV light irradiation, as (C_t) depicts the concentration time in MB and (C_0) is the initial concentration and b) the degradation of MB using TiO_2 thin film

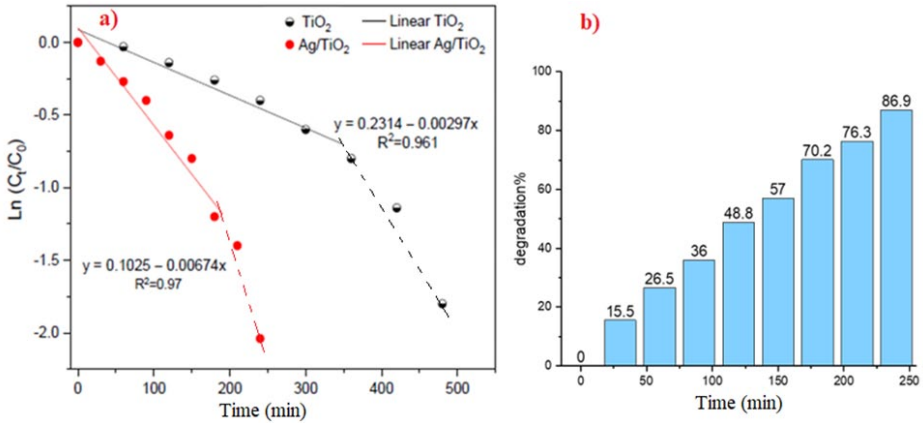

Fig. 7. a) Fitting ln (C_t/C_0) vs. (t) for experiments, as (C_t) depicts the concentration of MB at time (t) and (C_0) is the initial concentration of MB; the inner figure is the value and equation of linear fitting showing first (1) and second (2) process regime and b) the degradation of MB using Ag–TiO_2 thin film

TABLE 4

Different studies about the degradation of Methylene blue with light source, irradiation time, catalyst type and degradation ratio

No.	Catalyst	Catalyst type	Light source	Irradiation time (min)	Degradation (%)	Ref
1	Cr-TiO_2	Powders	UV	120	24.00	[70]
2	TiO_2	Pellets	UV	60	87.00	[71]
3	Ni-TiO_2	Powders	UV	240	96.00	[72]
4	6Ni-4Cr/TiO_2	Nanotubes	Sunlight	90	95.60	[73]
5	Fe-TiO_2/zeolite H-A	Powders	UV	50	87.87	[74]
6	Ag@ZnO/TiO_2	Nanocomposite	UV	60	99.85	[75]
7	TiO_2	Thin film	UV	240	92.00	[76]
8	TiO_2	Thin film	UV	300	82.20	[77]
9	Ag-TiO_2	Thin film	UV	240	86.90	This study

shows the advantages of this work over other works and gives a comparison of the degradation efficiency of some types of catalysts [81] as a function of photocatalytic activity [82] under different light sources [83,84]. Based on the above experimental results, we have highlighted the thin film type of catalyst as a clean and controllable synthesis process that cannot dissolve in the used waters.

4. Conclusion

Pure TiO_2 and Ag–doped TiO_2 thin film photocatalysts are successfully manufactured by dip coating method and films were deposited on glass substrates and annealed at calcination temperature of 400°C. XRD analysis shows that the prepared nanostructures are crystallize and they have the anatase-like structure. The crystal sizes of the annealed Ag–TiO_2 and the TiO_2 thin films are summarized through the XRD pattern as 29±1 and 23±1 nm for TiO_2 and Ag–TiO_2, respectively. This grain size leads to a large active surface area for organic molecules which render more adsorption sites, and therefore maximized photodegradation. Ag-doped TiO_2 sol-gel films showed improved photodegradation activities at low concentrations of methylene blue (3×10^{-5} M) in aqueous solutions compared to pure TiO_2 sol-gel films. The reaction kinetics followed a first order and half order Langmuir-Hinshelwood model for methylene blue (MB) concentrations of (3×10^{-5} M). For these concentrations, the global pseudo-first order reaction constant k_{app} goes from less than 1.4×10^{-3} min^{-1} for TiO_2 films to 5.4×10^{-3} min^{-1} for those of Ag–TiO_2. This means that the Ag–TiO_2 thin films had a k_{app} value which is 4 times higher than that of the TiO_2 thin films. The increased activity is due to the role of the incorporation of Ag in the formation of reactive oxygen species. The energy bandgap of the pure TiO_2 photocatalyst is about 3.3 eV, while that of the Ag–TiO_2 photocatalyst is 3.02 eV.

REFERENCES

[1] Z.H. Jabbar, S.E. Ebrahim, Recent advances in nano-semiconductors photocatalysis for degrading organic contaminants and microbial disinfection in wastewater: A comprehensive review. Environ. Nanotechnol. Monit. Manag. **17**, 100666 (2022).

[2] Y. Absalan, M.R. Razavi, M. Gholizadeh, A. Ahmadpour, S. Poursabagh, O. Kovalchukova, Enhance the photocatalytic performance of TiO_2 nano-semiconductor by simultaneously doping of transition and lanthanide elements for the C-C homocoupling reaction under sunlight irradiation. Nano-Structures & Nano-Objects. **30**, 100858-100875 (2022).

[3] O. Sacco, A. Mancuso, V. Venditto, S. Pragliola, V. Vaiano, Behavior of N-Doped TiO_2 and N-Doped ZnO in Photocatalytic Azo Dye Degradation under UV and Visible Light Irradiation: A Preliminary Investigation. Catalysts. **12**, 1208 (2022).

[4] J. Arun, S. Nachiappan, G. Rangarajan, R.P. Alagappan, K.P. Gopinath, E. Lichtfouse, Synthesis and application of titanium dioxide photocatalysis for energy, decontamination and viral disinfection: a review. Environ Chem Lett. **21**, 339-362 (2023).

[5] K. Shan, Z.Z. Yi, X.T. Yin, D. Dastan, F. Altaf, H. Garmestani, F.M. Alamgir, Mixed Conductivity Evaluation and Sensing Characteristics of Limiting Current Oxygen Sensors. Surf. Interfaces **21**, 100762 (2020).

[6] Z. Meiyu, Z. Shi, J. Zhang, K. Zhang, L. Lei, D. Dastan, B. Dong, Greatly Enhanced Dielectric Charge Storage Capabilities of Layered Polymer Composites Incorporated with low loading fractions of Ultrathin Amorphous Iron Phosphate Nanosheets. J. Mater. Chem. C. **9**, 10414 (2021).

[7] M. Fathinezhad, M.A.Tarighat, D. Dastan, Chemometrics heavy metal content clusters using electrochemical data of modified carbon paste electrode. Environ. Nanotechnol. Monit. Manag. **14**, 1003 (2020).

[8] S. Xia, Z. Shi, L. Sun, S. Sun, D. Dastan, R. Fan, Suppressing the loss and enhancing the breakdown strengths of high-k materials via constructing layered structure. Mater. Lett. **312**, 131654 (2022).

[9] M. Haghnegahdar, M.A. Tarighat, D. Dastan, Curcumin-functionalized nanocomposite AgNPs/SDS/MWCNTs for electrocatalytic simultaneous determination of dopamine, uric acid, and guanine in co-existence of ascorbic acid by glassy carbon electrode. J. Mater. Sci.: Mater. Electron. **32**, 5602-5613 (2021).

[10] I. Ashraf, S. Ahmad, D. Dastan, C. Wang, H. Garmestani, M. Iqbal, Fabrication of ionic liquid based D-Ti_3C_2/MoO_3 hybrid electrode system for efficient energy storage applications. Electrochimica Acta, **429**, 141036 (2022).

[11] Y. Liu, X. Wang, J. Shang, W. Xu, M. Sheng, C. Ye, The positive effect of formaldehyde on the photocatalytic renoxification of nitrate on TiO_2 particles. Atmos. Chem. Phys. **22**, 11347-11358 (2022).

[12] H. Yang, B. Yang, W. Chen, J. Yang, Preparation and Photocatalytic Activities of TiO_2-Based Composite Catalysts. Catalysts **12**, 1263 (2022).

[13] D.B. Miklos, C. Remy, M. Jekel, K.G. Linden, J.E. Drewes, U. Hübner, Evaluation of advanced oxidation processes for water and wastewater treatment – A critical review. Water Research. **139**, 118-131 (2018).

[14] S. Hisaindee, M.A. Meetani, M.A. Rauf, Application of LC-MS to the analysis of advanced oxidation process (AOP) degradation of dye products and reaction mechanisms. Trends Analyt. Chem. **49**, 31-44 (2013).

[15] M.C. Vagi, A.S. Petsas, Recent advances on the removal of priority organochlorine and organophosphorus biorecalcitrant pesticides defined by Directive 2013/39/EU from environmental matrices by using advanced oxidation processes: An overview (2007-2018). J. Environ. Chem. Eng. 102940 (2019).

[16] S. Malato, P. Fernández-Ibáñez, M.I. Maldonado, J. Blanco, W. Gernjak, Decontamination and disinfection of water by solar photocatalysis: Recent overview and trends. Catal. Today. **147**, 1-59 (2009).

[17] K. Nakata, A. Fujishima, TiO_2 photocatalysis: Design and applications. J. Photochem. Photobiol. C: Photochem. Rev. **13**, 169-189 (2012).

[18] S. Chiron, A. Fernandez-Alba, A. Rodriguez, E. Garcia-Calvo, Pesticide chemical oxidation: state-of-the-art. Water Res. **34**, 366-377 (2000).

[19] A.K. Al-Mousoi, M.K.A. Mohammed, R. Pandey, J. Madan, D. Dastan, G. Ravi, P. Sakthivele, G. Anandha Babu, Simulation and analysis of lead-free perovskite solar cells incorporating cerium oxide as electron transporting layer. RSC Adv. **12**, 32365 (2022).

[20] D. Dastan, S.L. Panahi, A. Yengantiwar, A.G. Banpurkar, Morphological and electrical studies of titania powder and films grown by aqueous solution method. Adv. Sci. Lett. **22**, 950-953 (2016).

[21] W.D. Zhou, D. Dastan, X. Yin, S. Nie, S. Wu, Q. Wang, J. Li, Optimization of gas sensing properties of n-SnO2/pxCuO sensors for homogenous gases and the sensing mechanism. J. Mater. Sci.: Mater. Electron. **31**, 18412-18426 (2020).

[22] A. Jayakrishnan, J. Silva, K. Kamakshi, D. Dastan, V. Annapureddy, M. Pereira, K. Sekhar, Are lead-free relaxor ferroelectric materials the most promising candidates for energy storage capacitors? Prog. Mater. Sci. **132**, 101046 (2023).

[23] X.T. Yin, J. Li, Q. Wang, D. Dastan, Z.C. Shi, N. Alharbi, H. Garmestani, X.M. Tan, Y. Liu, X.G. Ma, Opposite Sensing Response of Heterojunction Gas Sensors Based on SnO_2–Cr_2O_3 Nanocomposites to H_2 against CO and Its Selectivity Mechanism. Langmuir **37**, 13548-13558 (2021).

[24] X.T. Yin, S.S. Wu, D. Dastan, S. Nie, Y. Liu, Z.G. Li, Y.W. Zhou, J. Li, A. Faik, K. Shan, Z. Shi, M.A. Tarighat, X.G. Ma, Sensing Selectivity of SnO2-Mn3O4 Nanocomposite Sensors for the Detection of H_2 and CO Gases. Surf. Interfaces. **25**, 101190 (2021).

[25] D. Dastan, Studies on Electrical Properties of Hybrid Polymeric Gate Dielectric for Field Effect Transistors. Macromol. Symp. **347**, 81-86 (2015).

[26] J.P.B. Silva, K.C. Sekhar, R.F. Negrea, C. Ghica, D. Dastan, M.J.M. Gomes, Ferroelectric properties of ZrO_2 films deposited on ITO-coated glass. Ceram. Int. **48**, 6131-6137 (2022).

[27] M. Han, Z. Shi, W. Zhang, K. Zhang, H. Wang, D. Dastan, R. Fan, Significantly Enhanced High Permittivity and Negative Permittivity in Ag/Al_2O_3/3D-$BaTiO_3$/epoxy Metacomposites with Unique Hierarchical Heterogeneous Microstructures. Compos. – A: Appl. Sci. Manuf. **149**, 106559 (2021).

[28] L. Liang, Z. Shi, X. Tan, S. Sun, M. Chen, D. Dastan, B. Dong, L. Cao, Largely Improved Breakdown Strength and Discharge Efficiency of Layer-Structured Nanocomposites by Filling with a Small Loading Fraction of 2D Zirconium Phosphate Nanosheets. Adv. Mater. Interfaces **9**, 2101646 (2021).

[29] I. Ashraf, S. Ahmad, F. Nazir, D. Dastan, Z. Shi, H. Garmestani, M. Iqbal, Hydrothermal synthesis and water splitting application of d-Ti_3C_2 MXene/V_2O_5 hybrid nanostructures as an efficient bifunctional catalyst. Int. J. Hydrog. Energy **47**, 27383-27396 (2022).

[30] M.J. Kartha, B.A. Reshi, P.S. Walke, D. Dastan, Morphological Study of Thin Films: Simulation and Experimental Insights using Horizontal Visibility Graph, Ceram. Int. **48**, 5066-5074 (2021).

[31] S. Wei, Z. Shi, W. Wei, H. Wang, D. Dastan, M. Huang, J. Shi, S. Chen, Facile preparation of ultralight porous carbon hollow nanoboxes for electromagnetic wave absorption. Ceram. Int. **47**, 28014-28020 (2021).

[32] F. Altaf, S. Ahmed, D. Dastan, R. Batool, Z.U. Rehman, Z. Shi, M.U. Hameed, P. Bocchetta, K. Jacob, Novel sepiolite reinforced emerging composite polymer electrolyte membranes for high-performance direct methanol fuel cells. Mater. Today Chem. **24**, 100843 (2022).

[33] D. Dastan, A. Banpurkar, Solution processable sol-gel derived titania gate dielectric for organic field effect transistors. J. Mater. Sci. Mater. Electron. **28**, 3851-3859 (2016).

[34] Y. Panahi, H. Mellatyar, M. Farshbaf, Z. Sabet, T. Fattahi, A. Akbarzadehe, Biotechnological applications of nanomaterials for air pollution and water/wastewater treatment. Mater. Today: Proc. **5**, 15550-15558 (2018).

[35] I.S. Yunus, H.A. Kurniawan, D. Adityawarman, A. Indarto, Nanotechnologies in water and air pollution treatment. Environ. Technol. Rev. **1**, 136-148 (2012).

[36] A. Timoumi, H.M. Albetran, H.R. Alamri, S.N. Alamri, I.M. Low, Impact of annealing temperature on structural, morphological and optical properties of GO-TiO_2 thin films prepared by spin coating technique. Superlattices Microstruct. **139**, 106423 (2020).

[37] M.A. Ansari, H.M. Albetran, M.H. Alheshibri, A. Timoumi, N.A. Algarou, S. Akhtar, Y. Slimani, M.A. Almessiere, F.S. Alahmari, A. Baykal, I.M. Low, Synthesis of Electrospun TiO_2 Nanofibers and Characterization of Their Antibacterial and Antibiofilm Potential against Gram-Positive and Gram-Negative Bacteria. Antibiotics **9**, 572 (2020).

[38] O. Akhavan, Lasting antibacterial activities of Ag–TiO2/Ag/a-TiO2 nanocomposite thin film photocatalysts under solar light irradiation. J. Colloid Interface Sci. **336**, 117-124 (2009).

[39] Q.Q. Chu, Z. Sun, Y. Liu, H. Cui, B. Cheng, D. Dastan, K. Moon, G.J. Yang, C.P. Wong, Difluorobenzylamine Treatment of Organolead Halide Perovskite Boosting High Efficiency and Stable Photovoltaic Cells. ACS Appl. Mater. Interfaces, **14**, 11388-11397 (2022).

[40] S. Goulart, L.J. Jaramillo Nieves, A.G. Dal Bó, A.M. Bernardin, Sensitization of TiO_2 nanoparticles with natural dyes extracts for photocatalytic activity under visible light. Dyes and Pigments **182**, 108654 (2020).

[41] F. Orudzhev, S. Ramazanov, D. Sobola, A. Isaev, C. Wang, A. Magomedova, M. Kadiev, K. Kaviyarasu, Atomic Layer Deposition of Mixed-Layered Aurivillius Phase on TiO_2 Nanotubes: Synthesis, Characterization and Photoelectrocatalytic Properties. Nanomaterials **10**, 2183 (2020).

[42] E.C.R. Lopez, Rational Selection of Transition Metal Co-Dopant in Sulfur-Doped Titanium Dioxide. Eng. Proc. **5**, (2023).

[43] A. Timoumi, W. Zayoud, A. Sharma, M. Kraini, N. Bouguila, A. Hakamy, N. Revaprasadu, S. Alaya, Impact of thermal annealing inducing oxidation process on the crystalline powder of In_2S_3. J. Mater. Sci. Mater. Electron. **31**, 13636-13645 (2020).

[44] C. Chen, X. Li, W. Ma, J. Zhao, H. Hidaka, N. Serpone, Effect of transition metal ions on the TiO_2-assisted photodegradation of dyes under visible irradiation: a probe for the interfacial electron transfer process and reaction mechanism. J. Phys. Chem. B. **106**, 318-324 (2002).

[45] B. Jamoussi, R. Chakroun, A. Timoumi, K. Essalah, Synthesis and characterization of new imidazole phthalocyanine for photodegradation of micro-organic pollutants from sea water. Catalysts **10**, 906 (2020).

[46] O. Rosseler, M.V. Shankar, M.K. Du, L. Schmidlin, N. Keller, V. Keller, Solar light photocatalytic hydrogen production from water over Pt and Au/TiO_2 (anatase/rutile) photocatalysts: Influence of noble metal and porogen promotion. J. Catal. **269** (1), 179-190 (2010).

[47] T.L. Thompson, J.T. Yates, Surface science studies of the photoactivation of TiO_2 new photochemical processes. Chem. Rev. **106**, 4428-4453 (2006).

[48] A. Fujishima, X. Zhang, D.A. Tryk, TiO_2 photocatalysis and related surface phenomena. Surf. Sci. Rep. **63**, 515-582 (2008).

[49] V.K. Sharma, R.A. Yngard, Y. Lin, Silver nanoparticles: green synthesis and their antimicrobial activities. Adv. Colloid. Interfac. Sci. **145**, 83-96 (2009).

[50] S.X. Liu, Z.P. Qu, X.W. Han, C.L. Sun, A mechanism for enhanced photocatalytic activity of silver-loaded titanium dioxide, Catal. Today. **93**, 877-884 (2004).

[51] F. Bensouici, T. Souier, A.A. Dakhel, A. Iratni, R. Tala-Ighil, M. Bououdina, Synthesis, characterization and photocatalytic behavior of Ag doped TiO_2 thin film, Superlattices Microstruct. **85**, 255-265 (2015).

[52] A. Ferreira da Silva, I. Pepe, James L. Gole, S.A. Tomás, R. Palomino, W.M. de Azevedo, E.F. da Silva, R. Ahuja, C. Persson, Optical properties of in situ doped and undoped titania nanocatalysts and doped titania sol–gel nanofilms. Appl. Surf. Sci. **252**, 5365-5367 (2006).

[53] V. Vamathevan, R. Amal, D. Beydoun, G. Low, S. McEvoy, Photocatalytic oxidation of organics in water using pure and silver-modified titanium dioxide particles. J. Photochem. Photobiol. A: Chem. **148**, 233-245 (2002).

[54] N. Shimizu, C. Ogino, M.F. Dadjour, T. Murata, Sonocatalytic degradation of methylene blue with TiO_2 pellets in water, Ultrason. Sonochem. **14**, 184-190 (2007).

[55] A. Timoumi, S.N. Alamri, H. Alamri, The development of TiO_2 graphene oxide nano composite thin films for solar Cells. Results Phys. **11**, 46-51 (2018).

[56] W. Belhadj, A. Timoumi, F.A. Alamer, O.H. Alsalmi, S.N. Alamri, Experimental study and theoretical modeling of coating-speed-dependent optical properties of TiO_2-graphene-oxide thin films. Results Phys. **30**, 104867 (2021).

[57] D. Dastan, K. Shan, A. Jafari, T. Marszalek, M.K.A. Mohammed, L. Tao, Z. Shi, Y. Chen, X.T. Yin, N.D. Alharbi, F. Gity, S. Asgary, M. Hatamvand, L. Ansari, Influence of heat treatment on H_2S gas sensing features of NiO thin films deposited via thermal evaporation technique. Mater. Sci. Semicond. Process. **154**, 107232 (2023).

[58] T. Abdelmajid, D. Dastan, B. Jamoussi, K. Essalah, O.H. Alsalmi, N. Bouguila, H. Abassi, R. Chakroun, Z. Shi, Ş. Ţălu, Experimental and Theoretical Studies on Optical Properties of Tetra(Imidazole) of Palladium (II) Phthalocyanine. Mol. **27**, 6151 (2022).

[59] S.-C. Jung, B.-H. Kim, S.-J. Kim, N. Imaishi, Y.-I. Cho, Characterization of a TiO_2 photocatalyst film deposited by CVD and its photocatalytic activity. Chem. Vap. Deposition. **11**, 137-141 (2005).

[60] D. Dumitriu, A.R. Bally, C. Ballif, P. Hones, P.E. Schmid, R. Sanjinés, F. Lévy, V.I. Pârvulescu, Photocatalytic degradation of phenol by TiO_2 thin films prepared by sputtering. Appl. Catal. B: Environ. **25**, 83-92 (2000).

[61] X. Yin, Selectivity sensing response of ZnO-xCo_3O_4 based sensor to CO against CH_4. Mater. Sci. Semicond. Process **149**, 106883 (2022).

[62] P. Hoyer, Formation of a titanium dioxide nanotube array. Langmuir. **12**, 1411-1413 (1996).

[63] P. Zhu, D. Dastan, L. Liu, L. Wu, Z. Shi, Q.Q. Chu, F. Altaf, M.K.A. Mohammed,. Surface wettability of various phases of titania thin films: Atomic-scale simulation studies. J. Mol. Graph. Model. **118**, 108335 (2023).

[64] D. Dastan, K. Shan, A. Jafari, F. Gity, X.T. Yin, Z. Shi, N.D. Alharbi, B.A. Reshi, W. Fu, Ş. Ţălu, L. Aljerf, H. Garmestani, L. Ansari, Influence of nitrogen concentration on electrical, mechanical, and structural properties of tantalum nitride thin films prepared via DC magnetron sputtering. Appl. Phys. A, **128**, 400 (2022).

[65] A. Timoumi, H. Bouzouita, Thickness dependent physical properties of evaporated In2S3 films for photovoltaic application. Int. J. Renew. Energy Technol. Res., **2**, 188-195 (2013).

[66] M.K.A. Mohammed, A.K. Al-Mousoi, S. Singh, U. Younis, A. Kumar, D. Dastan, G.R. Mohammed, Ionic Liquid Passivator for Mesoporous Titanium Dioxide Electron Transport Layer to Enhance Efficiency and Stability of Hole Conductor-Free Perovskite Solar Cells. Energ. Fuel. **36**, 12192-12200 (2022).

[67] A. Soleimany, S. Khoee, D. Dastan, Z. Shi, S. Yu, B.S. Soleimany, Two-photon photodynamic therapy based on FRET using tumor-cell targeted riboflavin conjugated graphene quantum dot. J. Photochem. & Photobiol. B: Biol. **238**, 112602 (2023).

[68] M.K.A. Mohammed, A.K. Al-Mousoi, S.M. Majeed, S. Singh, A. Kumar, R. Pandey, J. Madan, D.S. Ahmed, D. Dastan, Stable Hole-Transporting Material-Free Perovskite Solar Cells with Efficiency Exceeding 14% via the Introduction of a Malonic Acid Additive for a Perovskite Precursor. Energ. Fuel. **36**, 13187-13194 (2022).

[69] W. Li, R. Liang, A. Hu, Z. Huanga, Y.N. Zhou, Generation of oxygen vacancies in visible light activated one-dimensional iodine TiO_2 photocatalysts. RSC Adv. **4**, 36959-36966 (2014).

[70] X.T. Yin, H. Huang, J.L. Xie, D. Dastan, J. Li, Y. Liu, X.M. Tan, X.C. Gao, W.A. Shah, X.G. Ma, High-performance visible-light active Sr-doped porous $LaFeO_3$ semiconductor prepared via sol–gel method. Green Chem. Lett. Rev. **15**, 546-556 (2022).

[71] W. Zhou, W. Li, J.Q. Wang, Y. Qu, Y. Yang, Y. Xie, K. Zhang, L. Wang, H. Fu, D. Zhao, Ordered Mesoporous Black TiO_2 as Highly Efficient Hydrogen Evolution Photocatalyst. J. Am. Chem. Soc. **136**, 9280-9283 (2014).

[72] Y. Wang, X. Zhang, J. Liu, Y. Wang, D. Duan, C. Fan,, Facile regeneration and photocatalytic activity of CuO-modified silver bromide photocatalyst. Mater. Sci. Semicond. Process. **40**, 613-620 (2015).

[73] C. Yu, G. Li, S. Kumar, H. Kawasaki, R. Jin, Stable Au25 (SR) 18/TiO_2 Composite Nanostructure with Enhanced Visible Light Photocatalytic Activity. J. Phys. Chem. A. **4**, 2847-2852 (2013).

[74] C. An, S. Peng, Y. Sun, Facile Synthesis of Sunlight-Driven AgCl:Ag Plasmonic Nanophotocatalyst. Adv. Mater. **22**, 2570-2574 (2010).

[75] S. Abbasi, D. Dastan, Ş. Ţălu, M. B. Tahir, Md. Elias, L. Tao, Z. Li, Evaluation of the dependence of methyl orange organic pollutant removal rate on the amount of titanium dioxide nanoparticles in MWCNTs-TiO_2 photocatalyst using statistical methods and Duncan's multiple range test. Int. J. Environ. An. Chem. (2022).

[76] F. Li, Y. Zhao, Y. Liu, Y. Hao, R. Liu, D. Zhao, Solution combustion synthesis and visible light-induced photocatalytic activity of mixed amorphous and crystalline $MgAl_2O_4$ nanopowders. J. Chem. Eng. **173**, 750-759 (2011).

[77] K.V. Kumar, K. Porkodi, F. Rocha, Langmuir-Hinshelwood kinetics – A theoretical study. Catal. Commun. **9**, 82-84 (2008).

[78] T. Zhang, T. Oyama, A. Aoshima, H. Hidaka, J. Zhao, N. Serpone, Photooxidative N-demethylation of methylene blue in aqueous TiO_2 dispersions under UV irradiation. J. Photochem. Photobiol. A: Chem. **140**, 163-172 (2001).

[79] C. Xu, G.P. Rangaiah, X.S. Zhao, Photocatalytic Degradation of Methylene Blue by Titanium Dioxide: Experimental and Modeling Study. Ind. Eng. Chem. Res. **53**, 14641-14649 (2014).

[80] C. Tingting, G. Huajing, L. Guorong, P. Zhongsheng, W. Shifa, Y. Zao, W. Xianwen, Y. Hua, Preparation of core-shell heterojunction photocatalysts by coating CdS nanoparticles onto $Bi_4Ti_3O_{12}$ hierarchical microspheres and their photocatalytic removal of organic pollutants and Cr(VI) ions. Colloids Surf. A: Physicochem. Eng. Asp. **633**, 127918 (2022).

[81] C. Peng, L. Fan, D. Hongzhi, C. Sheng, C. Lang, L. You-Ji, A. Chak-Tong, Y. Shuang-Feng, Porous double-shell CdS@C_3N_4 octahedron derived by in situ supramolecular self-assembly for enhanced photocatalytic activity. Appl. Catal. B: Environ. **252**, 33-40 (2019).

[82] T. Ningmei, L. Youji, C. Feitai, H. Zhenying, In situ fabrication of a direct Z-scheme photocatalyst by immobilizing CdS quantum dots in the channels of graphene-hybridized and supported mesoporous titanium nanocrystals for high photocatalytic performance under visible light. RSC Adv. **8**, 42233-42245 (2018).

[83] X. Lin, Y. Li, F. Chen, P. Xu, M. Li, Facile synthesis of mesoporous titanium dioxide doped by Ag-coated graphene with enhanced visible-light photocatalytic performance for methylene blue degradation. RSC Adv. **7**, 25314-25324 (2017).

[84] S.M. Chaudhari, P.M. Gawal, P.K. Sane, S.M. Sontakke, P.R. Nemade, Solar light-assisted photocatalytic degradation of methylene blue with Mo/TiO_2: a comparison with Cr-and Ni-doped TiO_2. Res. Chem. Intermed. **44**, 3115-3134 (2018).